doi:10.1016/S0022-2836(02)00595-8 available online at http://www.idealibrary.com on IDEAL® J. Mol. Biol. (2002) 321, 517–526

JMB

Solution Structure of ω-Grammotoxin SIA, A Gating Modifier of P/Q and N-type Ca^{2+} Channel

Koh Takeuchi[1], Eun Ju Park[2], Chul Won Lee[2], Jae Il Kim[2] Hideo Takahashi[1,3], Kenton J. Swartz[4] and Ichio Shimada[1,3]*

[1]*Graduate School of Pharmaceutical Sciences The University of Tokyo, Tokyo 113-0033, Japan*

[2]*Kwangju Institute of Science and Technology, Kwangju 500-712, Korea*

[3]*Biological Information Research Center (BIRC) National Institute of Advanced Industrial Science and Technology (AIST), Aomi Koto-ku, Tokyo 135-0064 Japan*

[4]*Molecular Physiology and Biophysics Unit, National Institute of Neurological Disorders and Stroke, National Institute of Health, Bethesda MD 20892, USA*

**Corresponding author*

ω-Grammotoxin SIA (GrTx) is a 36 amino acid residue protein toxin from spider venom that inhibits P/Q and N-type voltage-gated Ca^{2+} channels by modifying voltage-dependent gating. We determined the three-dimensional structure of GrTx using NMR spectroscopy. The toxin adopts an "inhibitor cystine knot" motif composed of two β-strands (Leu19-Cys21 and Cys30-Trp32) and a β-bulge (Trp6, Gly7-Cys30) with a $+2x$, -1 topology, which are connected by four chain reversals. Although GrTx was originally identified as an inhibitor of voltage-gated Ca^{2+} channel, it also binds to K^+ channels with lower affinity. A similar cross-reaction was observed for Hanatoxin1 (HaTx), which binds to the voltage-sensing domains of K^+ and Ca^{2+} channels with different affinities. A detailed comparison of the GrTx and HaTx structures identifies a conserved face containing a large hydrophobic patch surrounded by positively charged residues. The slight differences in the surface shape, which result from the orientation of the surface aromatic residues and/or the distribution of the charged residues, may explain the differences in the binding affinity of these gating modifiers with different voltage-gated ion channels.

Keywords: calcium channel; gating modifier; grammotoxin; nuclear magnetic resonance; potassium channel

Introduction

Voltage-gated channels are expressed by many cells and play a crucial role in regulating membrane potential and various cellular functions. A variety of toxins isolated from scorpions, snakes, snails, and insects are known to inhibit voltage-gated channels. In many instances, these toxins interact quite selectively with specific channel types and thus have been useful pharmacological tools for investigating channel structure and function and for evaluating specific channels as targets for drug development. The structure determination of these toxins provides a foundation for investigating the molecular basis of toxin binding and selectivity and for the design of drugs affecting nervous system function.

Toxins that interact with voltage-gated ion channels can be distinguished into two basic types: pore blockers and gating modifiers. Pore blockers are thought to bind to the central pore region of the channel and to inhibit by physically occluding the ion-conducting pore.[1] The three-dimensional structures of many pore blockers have been determined using NMR.[2–9] Although pore-blocking toxins can interact with the same ion selective pores in channels with different gating mechanisms,[10] they do not cross-react between channels with different ion selectivity filters. It is therefore not surprising that few

Abbreviations used: DQF-COSY, double-quantum-filtered correlated spectroscopy; E.COSY, exclusive-COSY; FAB-MASS, fast atom bombardment mass spectrometry; GrTx, ω-grammotoxin SIA; HaTx, hanatoxin; HOHAHA, homonuclear Hartmann–Harn; HPLC, high-pressure liquid chromatography; NMR, nuclear magnetic resonance; NOE, nuclear Overhauser effect; NOESY, nuclear Overhauser effect spectroscopy.

E-mail address of the corresponding author: shimada@iw-nmr.f.u-tokyo.ac.jp

0022-2836/02/$ - see front matter

structural similarities exist between pore blockers that interact with channels containing different ion selectivity filters.[11–19]

A number of gating modifier toxins target the voltage-sensing region within the extracellular border of the channels α-subunit and alter voltage-dependent gating.[20–24] The structures of several Na^+ channel gating modifiers including the α and β-scorpion toxins and the sea anemone toxins have been determined.[25,26] As for the K^+ channel, the structure of Hanatoxin1 (HaTx), a gating modifier of the *drk1* K^+ channel,[20,27] was determined in our previous study.[28] A comparison of the structures of the Na^+ and K^+ channel gating modifiers suggests that a conserved motif, consisting of a hydrophobic patch surrounded by positively charged residues, may be functionally important for the binding activity of these gating modifiers.[25,26,28]

ω-Grammotoxin SIA (GrTx) is a 36-amino-acid gating modifier that was first identified as an inhibitor of the P/Q and N-type voltage-gated Ca^{2+} channels.[27,29–31] However, GrTx is closely related to HaTx (42% sequence identity) and both toxins cross-reactive with Ca^{2+} and K^+ channels.[32] Mapping studies in the *drk1* voltage-gated K^+ channel suggest that both GrTx and HaTx interact with the C terminus of S3, a region that is conserved in several repeats of both P/Q and N-type Ca^{2+} channels.[21,32] Although these observations argue for a common binding site on the K^+ and Ca^{2+} channels, the affinities of GrTx and HaTx for these channels vary considerably. The binding constant of HaTx to the K^+ channel is about 200-fold higher than that of GrTx, whereas GrTx binds to the Ca^{2+} channel with much higher affinity than HaTx.[32] A comparison of the three-dimensional structures of these two toxins would help one to clarify the structural basis of this interesting cross-reactivity and selectivity. In the present study, we determined the solution structure of GrTx using proton nuclear magnetic resonance (^{1}H-NMR) spectroscopy along with dynamical simulated annealing calculations. On the basis of the structure, we discuss the structure–function relationships between GrTx and HaTx to better understand their different selectivities for voltage-gated ion channels.

Results and Discussion

Characterization of synthetic GrTx

We studied the interaction of synthetic GrTx with the α_{1A} voltage-activated calcium channel expressed in *Xenopus oocytes* using two-electrode voltage clamp recording techniques. The calcium channel was activated by moderate strength depolarization of the membrane, repeated at ten-second intervals, before and after adding the toxin to the recording chamber. At a concentration of 200 nM, synthetic GrTx produced complete inhibition of calcium channel currents elicited by depolarization to −15 mV (Figure 1(a), left). Even with these relatively high toxin concentrations, the onset of inhibition by the toxin was rather slow, occurring with a time constant of ~30 seconds (Figure 1(b)). Lower concentrations of toxin (25 nM) inhibited the calcium channel by 90%, but with much slower kinetics (τ_{on} ~ 200 seconds). The slow apparent binding kinetics observed with sub-saturating concentrations of toxin made it very difficult to reach equilibrium and therefore to examine the concentration dependence for inhibition by the toxin. Nevertheless, the extent of inhibition observed at 25 nM indicates that the binding affinity of the synthetic toxin must be in the low nM range or less. Similar results have been observed with GrTx inhibition of native calcium channels.[31]

Like other gating modifier toxins, GrTx is known to inhibit voltage-activated calcium channels by shifting activation to more depolarized voltages. One rather unique hallmark of GrTx is that calcium channel currents elicited by strong depolarization can be larger in the presence of the toxin when compared to control conditions, possibly due to an increased maximal open probability for the toxin bound channel.[31] Figure 1(c) shows the voltage dependence for the effects of synthetic GrTx on the α_{1A} calcium channel. While the toxin produced complete inhibition of the channel at negative voltages (−30 to +40 mV), large depolarizations (+100 mV) resulted in macroscopic currents through the toxin bound channels that are larger than recorded for control channels. In addition, the activation kinetics following strong depolarizations were significantly slower for the toxin bound channels (Figure 1(a), right). All of these voltage-dependent properties are similar to those previously reported for the interaction between GrTx and native P-type calcium channels.[31]

Structure calculations

We established the sequence-specific resonance assignments for all of the observed protons in GrTx according to standard method for small proteins.[33] On the basis of the established sequence-specific assignments, we carefully analyzed the NOE cross-peaks on the NOESY spectra and translated them into four classes of 536 distance constraints for the structural calculations. In addition, three distance constraints for disulfide bonds and ten distance constraints relating to hydrogen bonds, which were unambiguously determined in the initial runs of the structural calculations, were also used in the structural calculation. The disulfide bond patterns were determined to be Cys2-Cys16, Cys9-Cys21, and Cys15-Cys30, which are the most agreeable with the experimental data and the most rationally folded without serious bad contact. For the hydrogen bonds, out of the 11 slowly exchanging protons

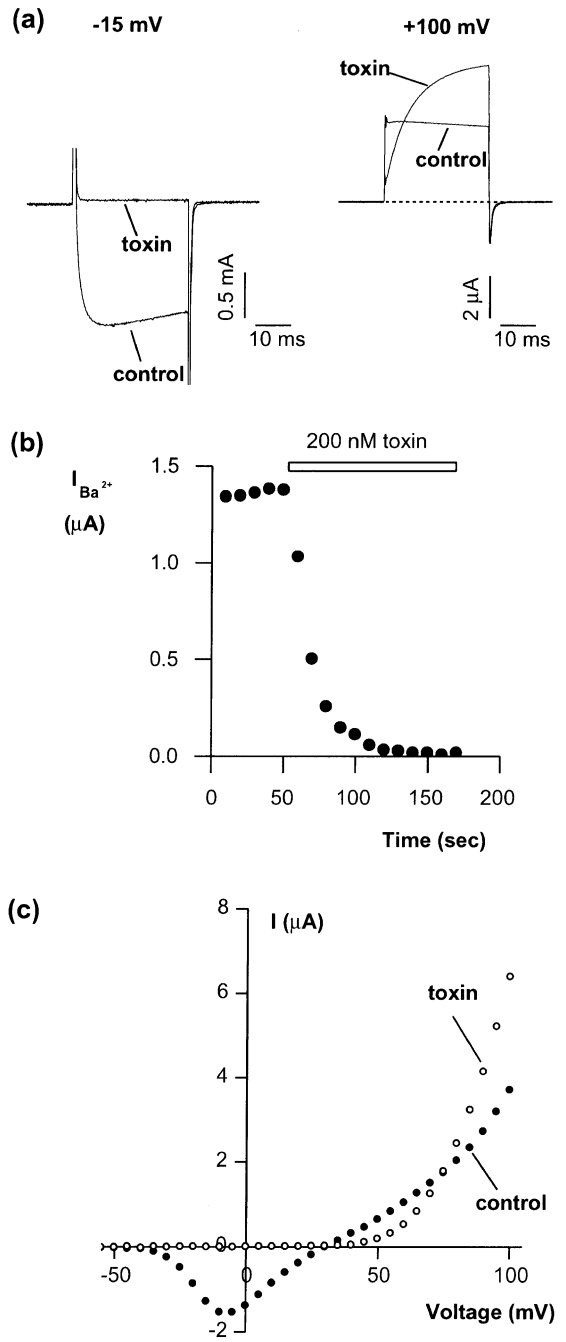

Figure 1. Voltage-dependent inhibition of the α_{1A} calcium channel by synthetic GrTx. (a) Currents elicited by depolarization to −15 mV (left) or +100 mV (right) in either the absence and presence of 200 nM GrTx. Extracellular charge carrier was 1 mM Ba^{2+} and intracellular charge carrier was endogenous K^+ (~100 mM). Leak and capacitive currents have been isolated and subtracted using 100 μM Cd to block Ca^{2+} channel currents. Holding voltage was −90 mV and tail voltage was −60 mV. (b) Time-course for inhibition by GrTx. Steady-state Ba^{2+} current elicited by depolarizations to −15 mV at 10-second intervals before and after the application of toxin. Inward Ba^{2+} currents were measured 10 ms after depolarization. Same cell as in (a). (c) Steady-state Ca^{2+} channel currents elicited by depolarization to various membrane voltages before and after the application of 200 nM GrTx. Current measurements were made 28 ms after depolarization. Same cell as in (a).

of the main chain amide groups that were observed in the hydrogen–deuterium (H–^{2}H) exchange experiments, five hydrogen-bonding pairs were unambiguously determined: (Cys9(HN)–Asn28(CO), Cys16(HN)–Val3(CO), Ala20(HN)–Val31(CO), Cys30(HN)–Gly7(CO), and Val31(HN)–Ala20(CO)). For the backbone ϕ torsion angles, 13 constraints were applied: three residues with $^3J_{N\alpha} < 5.5$ Hz (Cys2, Lys8, and Ser35) were constrained to $\phi = [-90°, -40°]$, and ten residues with $^3J_{N\alpha} > 8.0$ Hz (Cys9, Ser10, Cys16, Leu19, Ala20, Cys21, Ser23, Lys24, Cys30, and Val31) were constrained to $\phi = [-160°, -80°]$. For the χ^1 torsion angles seven constraints were used. The torsion angle for Ser35 fell to $\chi^1 = [0°, 120°]$, those for Cys16 and Pro17 fell to $\chi^1 = [120°, 240°]$, and the others (His18, Cys21, Trp25, and Trp32) fell to $\chi^1 = [-120°, 0°]$.

To determine the solution structure of GrTx, we carried out the simulated annealing calculations starting with 100 initial random structures, and obtained 69 acceptable structures with no violations >0.5 Å for the distance constraint and >5.0° for the angle constraint. From these structures, we have chosen the 20 final converged structures with the lowest X-PLOR energy. The evaluated structural statistics for these 20 converged structures are summarized in Table 1. The low values of the Lennard-Jones van der Waals energy and the small deviations from the idealized covalent geometry indicate the absence of serious bad contact and distortion in the converged structures. Figure 2(a) shows the best-fit superposition of the backbone atoms (N, C^α, and C) for the 20 final converged structures. The N-terminal residue (Asp1), C-terminal segment (Asp33-Val36), and two loop regions (Ser10-Cys15 and Lys22-Asn28) showed some apparent deviations among the obtained structures. The remaining part of the structures and the disulfide bonds of Cys9-Cys21, Cys15-Cys30 were well defined, with root mean square differences of 0.27 Å for the backbone atoms and 0.96 Å for all heavy atoms. In the Ramachandran plot for the defined segments, 57.5% of the backbone dihedral angles fell in the most favored region and the remaining were in the generally allowed regions.

Description of structures

Figure 2(c) shows the ribbon representation of the secondary structures in GrTx. GrTx contains two β-strands (Leu19-Cys21 and Cys30-Trp32) and a "classic type" β-bulge structure at (Trp6, Gly7)-Cys30, which are stabilized by three disulfide bonds.[34] In the β-strands and the β-bulge structure, slow H–D exchange rates of the amide protons were observed for Ala20 and Asn31 and for Trp6, Gly7, and Cys30, respectively. These observations indicate the existence of the hydrogen-bond network within the structures. Considering the β-bulge as a modified β-strand, GrTx is classified into the topology of $+2x$, -1.[34] The topology of

Table 1. Structural statistics for the 20 lowest energy structures

RMS deviation from experimental distance constraints (Å)[a,b] (536)	0.018 ± 0.001
RMS deviation from experimental dihedral constraints (deg.)[a] (20)	0.907 ± 0.085
Energetic statistics (kcal/mol)[c]	
F_{NOE}	9.15 ± 0.83
F_{tor}	1.02 ± 0.19
F_{repel}	9.17 ± 0.57
$E_{L\text{-}J}$	−94.0 ± 12.1
RMS deviation from idealized geometry	
Bonds (Å)	0.002 ± 0.00004
Angles (deg.)	0.610 ± 0.005
Impropers (deg.)	0.439 ± 0.014
Ramachandran analysis (residues 2–9, 16–21, 29–32)[d]	
Most favored regions (%)	57.5
Additionally allowed regions (%)	52.5
Generously allowed regions (%)	0.0
Disallowed regions (%)	0.0
Average pairwise RMS difference (Å)	
Backbone (N, C^{α}, C) (residues 2–9, 16–21, 29–32)	0.27 ± 0.08
All heavy atoms (residues 2–9, 16–21, 29–32)	0.96 ± 0.20

None of these 20 structures exhibited distance violation >0.5 Å or dihedral angle violations >5°.

[a] The number of each experimental constraint used in the calculations is given in parentheses.

[b] Distance restraints consisted of 180 intraresidue, 151 sequential, 48 medium range ($2 \leq |i - j| \leq 4$), and 157 long range NOE restraints.

[c] F_{NOE}, F_{tor}, and F_{repel} are energies related to the NOE violations, the torsion angle violations, and van der Waals repulsion term, respectively. The values of the force constraints used for these terms are the standard values as depicted in the X-PLOR 3.1 Manual.[57] $E_{L\text{-}J}$ is the Lennard-Jones van der Waals energy calculated with the CHARMm empirical energy function.[63] $E_{L\text{-}J}$ was not used in the dynamical simulated annealing calculations.

[d] The program PROCHECK-NMR[61] was used to assess the stereochemical quality of the structures.

$+2x$, -1 is also observed in the Ca^{2+} channel pore blocker ω-conotoxins[5–10] or the Ca^{2+} channel gating modifier ω-agatoxins,[35–38] but is distinct from the two β-stranded motif observed for the K^{+} channel gating modifier HaTx,[28] all of which have the same disulfide bonding patterns similar to GrTx.

In GrTx, there are four chain reversals, the segments of Arg4-Gly7 (turn 1), Gln11-Asp14 (turn 2),

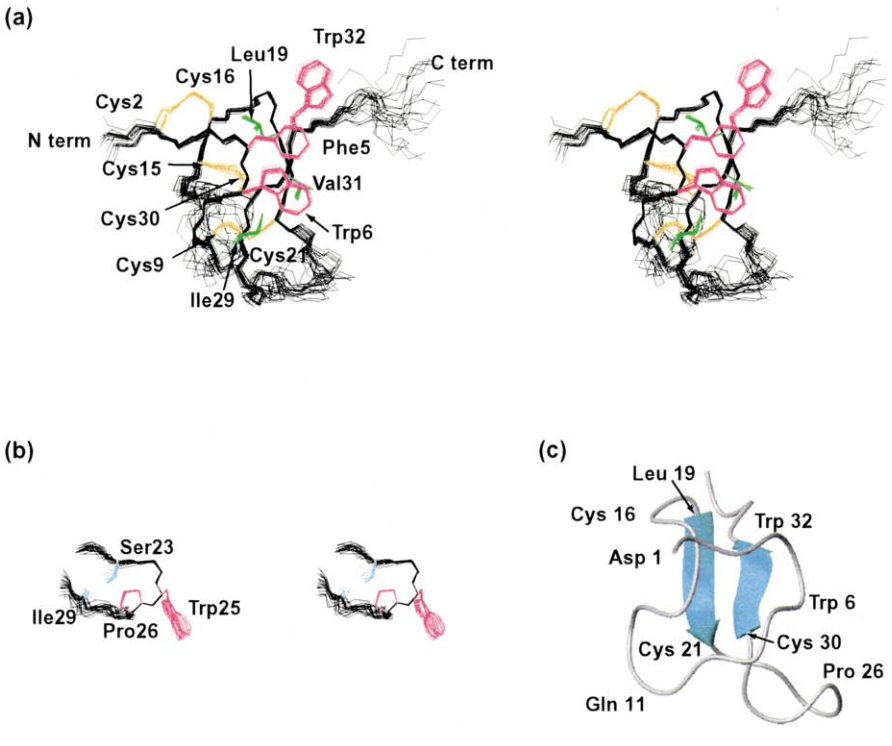

Figure 2. Converged structures of GrTX. (a) Stereo pairs of the backbone heavy atoms (N, C^{α}, and C) for the 20 final converged structures. These are the best-fit superpositions of the backbone heavy atoms for the central part (residues 2–9, 16–21, and 29–32) of the molecules. The side-chains of the cysteine residues are shown and colored in orange. The side-chains of the central core residues (Leu19, Ile29, and Val31), and the surface aromatic residues (Phe5, Trp6, and Trp32) are also represented in green and magenta, respectively. (b) Stereo pairs of the backbone heavy atoms (N, C^{α}, and C) for the loop from residues 22–29. These are the best-fit superpositions of the backbone heavy atoms for the turn 3 segment (residues 23–26). The side-chains of two hydrophobic residues (Trp25 and Pro26) are also represented in magenta. The side-chain of Ser23 and the amide group of Ile29, which make hydrogen bond within the loop region, are represented in cyan. (c) Ribbon representation of the backbone peptide folding of GrTx (the lowest X-PLOR-energy structure). The structure topology of the double-stranded antiparallel β-sheet was identified by MOLMOL.[62]

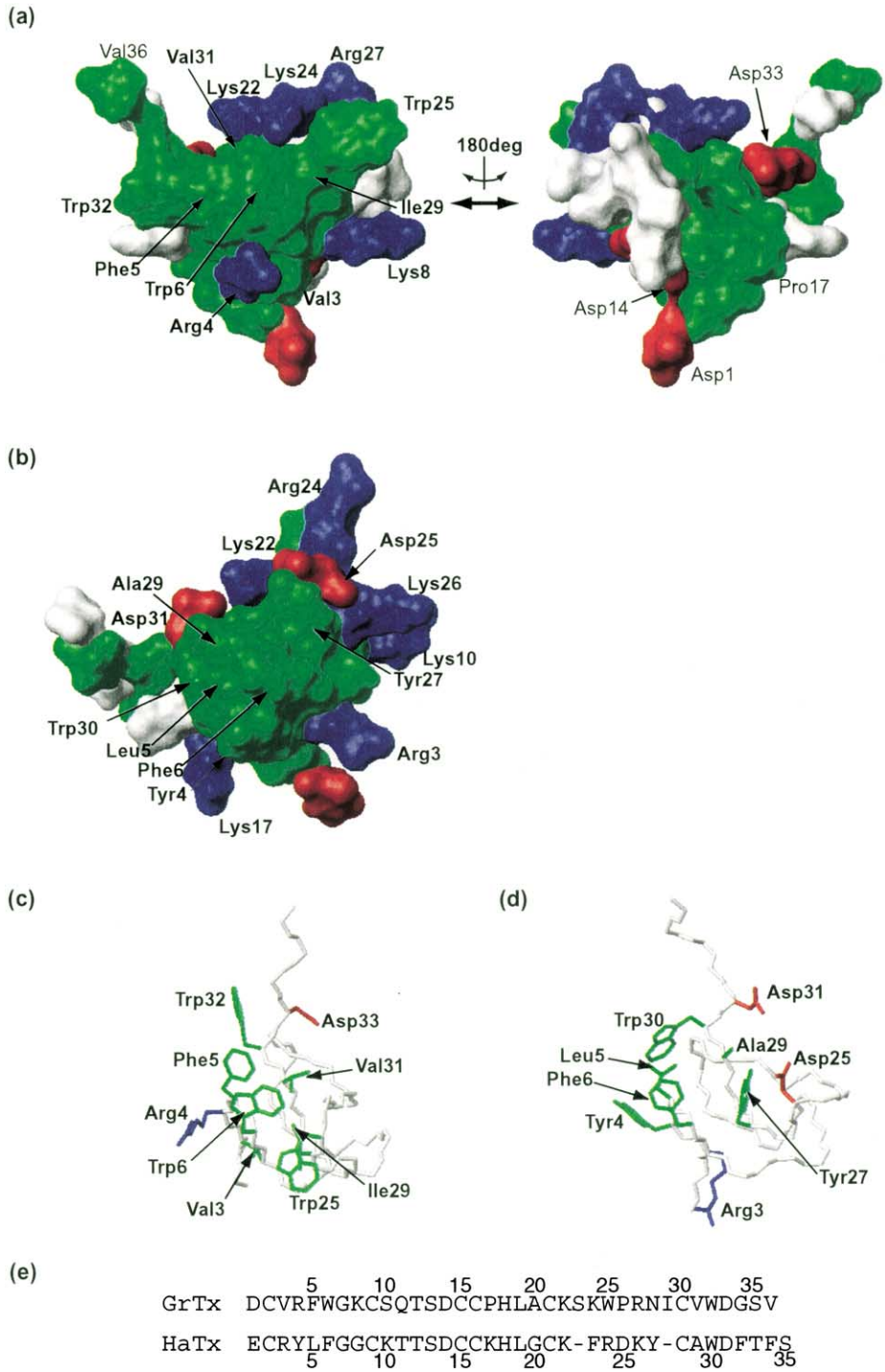

Figure 3. Comparisons of the structures between GrTx and HaTx. (a) Surface profiles of GrTx. The left and right Figures are the 180° rotations about the vertical axis relative to each other. (b) Surface profile of HaTx.[28] Comparison of the hydrophobic patches and some interesting charged residues between (c) GrTx and (d) HaTx. Hydrophobic residues (Ala, Cys, Gly, Ile, Leu, Phe, Pro, Trp, Tyr, and Val) are colored in green, and basic (Arg and Lys) and acidic (Asp) residues are colored in blue and red, respectively. The other residues are colored in white. The residues in the hydrophobic patch and the surrounding charged residues are labeled and highlighted by bold characters. Other highly exposed residues are also indicated. (e) Comparative arrangements of the amino acid sequences of GrTx and HaTx.

Cys16-Leu19 (turn 3), and Ser23-Pro26 (turn 4). Turn 1 is classified as type IV, a miscellaneous category. There is no hydrogen bonding within the turn conformation. Turn 2 is disordered and has no significant secondary structure. Turn 3 forms a type I β-turn, in which the average dihedral angles for Pro17 and His18 are $\psi_2 = -11°$, $\phi_3 = -89°$, and $\psi_3 = 14°$, respectively. In this turn, the Cys16 oxygen is hydrogen bonded to the Leu19 amide, and a slow H–^{2}H exchange rate of the Leu19

amide is observed in the H–^{2}H exchange experiment. Turn 4 is classified as type VII, with $\psi_2 = 35°$, and $\phi_3 = 172°$. Turn 4 is part of a long loop from Lys22 to Ile29. As shown in Figure 2(b), this loop fits well in the turn 4 segment, but the hinge-like disorder found in Lys22 and Asn28 does not define the relative position of the loop with respect to the other part of the molecule. In this loop, the Ser23 O^{γ} likely form a hydrogen bond between the amide proton of Ile29 in 13 of the 20 converged structures.

There are two more hydrogen bonds in the converged structures of GrTx, i.e. the hydrogen bond between the amide proton of Cys16 and the oxygen of Val3, and that between the oxygen of His18 and the amide proton of Asn33. The slow exchange rate for Cys16 and the relatively slow exchange rate for Asn33 support the existence of these hydrogen bonds. The hydrogen bond between the amide proton of Cys16 and the oxygen of Val3 stabilizes the N-terminal segment (Asp1-Arg4), together with the disulfide bridge between Cys2 and Cys16. The hydrogen bond between the oxygen of His18 and the amide proton of Asn33 fixes the orientation of the side-chain of Asn33, which is oriented opposite to the aromatic ring of Trp32.

In the converged structures of GrTx, two disulfide bridges Cys9-Cys21 and Cys15-Cys30, and the side-chains of residues Leu19, Ile29, and Val31 are well defined and form the hydrophobic core in GrTx. The orientations of the surface aromatic rings, i.e. the phenyl ring of Phe5 and the indole rings of Trp6 and Trp32, are also well determined. As shown in Figure 2(a), these aromatic rings are stacked in-line with each other and form a significant profile on the surface of GrTx. The phenyl ring of Phe5 has a "staggered" stacking on the indole ring of Trp6. The indole ring of Trp32 has a "tilted" stacking on the phenyl ring of Phe5. This "tilted" stacking induces an aromatic–aromatic interaction between the positively polarized hydrogen of Trp32 and the cloud of π-electrons of Phe5, which stabilizes the orientation of the two aromatic rings by ~1 kcal/mol.[39,40] The phenyl ring of Phe5 is also stacked on Leu19, and the indole ring of Trp6 is stacked on Ile29.

Surface profile of GrTx

Figure 3(a) shows the surface profile of GrTx. On the surface of GrTx, there exist five positively charged residues (Arg4, Lys8, Lys22, Lys24, and Arg27), three negatively charged residues (Asp1, Asp14, and Asp33), and interestingly, some hydrophobic residues that are highly exposed to the solvent (Val3, Phe5, Trp6, Pro17, Trp25, Trp32, and Val36, >30% of the side-chain is exposed). Most of these highly exposed hydrophobic residues (Val3, Phe5, Trp6, Trp25, and Trp32) are gathered on one surface of the structure (Figure 3(a), left), and compose a large hydrophobic patch with the partially exposed hydrophobic residues (Ile29, and Val31, >15% of the side-chain is exposed). Five basic residues (Arg4, Lys8, Lys22, Lys24, and Arg27) are arranged around the edge of the hydrophobic patch.

The clustering of the unusually exposed hydrophobic patch and the surrounding positively charged residues is a significant feature of the GrTx surface. In addition, there is no negatively charged residue on the same surface of the hydrophobic patch. The opposite side of GrTx is mainly composed of charged and polar residues, and has no remarkable structural features.

In the previous paper, we pointed out that the surface motif of a hydrophobic patch surrounded by positively charged residues on gating modifier toxins may be responsible for binding to voltage-dependent channels.[28] A comparison of the surfaces of GrTx and HaTx show that the hydrophobic patch and surrounding positively charged residues are conserved on both toxins. In addition, the special distributions within the motif are also well conserved (Figure 3(a) and (b)). For instance, Phe5, Trp6, Ile29, Val31, and Trp32 in GrTx occupy the corresponding places of Leu5, Phe6, Tyr27, Ala29, and Trp30 in HaTx, respectively. As for the basic residues, Lys22, Lys24, and Arg27 in GrTx are in the corresponding places of Lys22, Arg24, and Lys26 in HaTx. From this comparison, we suggest that the face of GrTx containing Phe5, Trp6, Lys22, Arg24, Arg27, Ile29, Val31, and Trp32 may interface directly with the voltage-sensing domains in voltage-gated channels.

Structure–function relationships between GrTx and HaTx

GrTx binds to P/Q and N-type voltage-gated Ca^{2+} channels with high affinity,[27,29–31] but binds to the *drkl* voltage-gated K^+ channel with low affinity. HaTx has an opposite selectivity, binding tightly to K^+ channels and weakly to Ca^{2+} channels.[32] Figure 3(c) and (d) shows a comparison of the orientations of residues within the hydrophobic patch on the surfaces of GrTx and HaTx that we propose interface with voltage-gated channels. The orientations of the side-chain of Trp32 in GrTx and that of Trp30, the corresponding residue in HaTx, are different. The χ^1 angle of Trp32 in GrTx is 139.9 ± 1.7°, while that of Trp30 in HaTx is −64.6 ± 5.8°. In GrTx, the aromatic–aromatic interaction and the atomic contact between Phe5 and Trp32 render the conformation of Trp32 an "open" conformation. Phe5 in GrTx is replaced with the hydrophobic but less bulky Leu5 residue in HaTx. In HaTx, the aromatic–aromatic interaction and the atomic contact found in GrTx are broken, and Trp30 takes a "closed" conformation that directly interacts with the Leu5. This conformational difference might result in the difference in binding affinities of GrTx and HaTx for voltage-gated ion channels.

The different binding affinities of GrTx and HaTx to K^+ and Ca^{2+} channels might also involve

small but significant difference in the distribution of the charged residues. For example, Val3, Arg4, and Trp25 in GrTx are replaced with Arg3, Tyr4, Asp25, respectively, in HaTx. Also, the orientation of the side-chain of Asp residues is different between Asp33 in GrTx and Asp31 in HaTx. As shown in Figure 3(a), left, these replacements lead to the loss of a negative charge and the addition of a positive charge on the surface of GrTx, compared to the equivalent region on HaTx.

Conclusion

In the present study, the three-dimensional structure of a gating modifier, GrTx, has been determined by NMR. We find that GrTx possesses a surface that is very similar to the face of HaTx that has previously been proposed to interface with the voltage-sensing domains in voltage-gated K^+ channels. The observed similarities between GrTx and HaTx are consistent with the observed cross-reactivity of these two toxins with voltage-gated K^+ and Ca^{2+} channels. A detailed comparison between GrTx and HaTx reveals that there are subtle, but significant, differences in the shape of the binding surface and the distribution of the charged residues in this region. These subtle structural differences may explain the different affinities of GrTx and HaTx for K^+ and Ca^{2+} channels.

Materials and Methods

Sample preparation

The linear precursor of GrTx was chemically synthesized by a solid-phase methodology and then was oxidized into the native folding as previously described.[29] The synthetic GrTx has the identical properties and potency as that purified from Chilean tarantula (*Grammostola spatulata*) venom.[41] The amino acid sequence of the linear precursor of GrTx (H_2N-DCVRFWGKCSQTSDCCPHLACKSKWPRNICVWDGSV-COOH) was confirmed by an amino acid analysis and a FAB-MASS measurement. The purity of the synthetic GrTx was confirmed by reverse phase HPLC.

Chemical reduction of GrTx indicated the presence of three disulfide bridges.[29] However, because of the difficulty in applying the methods using selective proteolysis, no information was available for the disulfide bridging pattern of GrTx.

Molecular biology

cDNAs encoding rabbit brain α_{1A} (BI-1),[42] rat brain β_{1b}[43] and rabbit skeletal muscle $\alpha_2\delta$[44] were kindly provided by Lutz Birnbaumer (UCLA, Los Angeles, CA) in the pAGA2 vector.[45] α_{1A} and $\alpha_2\delta$ were linearized with *Xho*I and β_{1b} was linearized with *Hin*dIII. All subunits were transcribed using T7 RNA polymerase.

Electrophysiology

Oocytes from *Xenopus laevis* frogs were removed surgically and incubated with agitation for 1.5 hours in a solution containing NaCl (82.5 mM), KCl (2.5 mM), $MgCl_2$ (1 mM), Hepes (5 mM), collagenase (2 mg/ml; Worthington Biochemical Corp.), pH 7.6 with NaOH. Defolliculated oocytes were injected with cRNA and incubated at 17 °C in a solution containing NaCl (96 mM), KCl (2 mM), $MgCl_2$ (1 mM), $CaCl_2$ (1.8 mM), Hepes (5 mM), gentamicin (50 μg/ml; Gibco BRL), pH 7.6 with NaOH for 1–7 days prior to electrophysiological recording. Approximately equal quantities (~10–100 ng) of cRNA for α_{1A}, β_{1b} and $\alpha_2\delta$ subunits were injected in each oocyte. Oocyte membrane voltage was controlled using an OC-725C oocyte clamp (Warner Instruments). Data were filtered at 2 kHz (8-pole Bessel) and digitized at 10 kHz. Microelectrode resistances were 0.1–0.8 MΩ when filled with 3 M KCl. Oocytes were studied in 160–200 μl recording chambers perfused with a solution containing $BaOH_2$ (1 mM), $NaCH_3SO_3$ (100 mM), Hepes (10 mM), pH 7.6 with NaOH. Contamination of Ca^{2+} activated Cl^- current was minimized by recording in Cl^- free solution and recording Ba^{2+} currents usually less than 2 μA (mostly ~1 μA). Agar salt bridges containing 1 M NaCl were used to connect the ground electrode pools and the recording chamber. All experiments were carried out at room temperature (~22–25 °C).

NMR experiments

For the NMR experiment, 4 mg of GrTx were dissolved in 400 μl of H_2O containing 10% (v/v) ^2H_2O adjusted to pH 3.5 with HCl. The final peptide concentration of the sample was 2.4 mM. NMR spectra were recorded on JEOL α-500 and Bruker DRX 600 spectrometers. All two-dimensional NMR experiments, i.e. DQF-COSY, E.COSY, HOHAHA, and NOESY, were performed using standard pulse sequences and phase cycling.[46–50] In a typical experiment, 800 increments of 2 K data points were recorded. For DQF-COSY and E.COSY, 4 K data points were recorded for an accurate estimation of the ^3J coupling. Spectral widths were 12 ppm. The HOHAHA spectrum was recorded at 283 K with a mixing time of 80 ms. The NOESY spectra were recorded at 283 K and 300 K with mixing times of 80 ms, 150 ms, and 250 ms. The HOHAHA and NOESY experiments include the Watergate scheme for water suppression.[51] The DQF-COSY and E.COSY experiments were carried out at 283 K using a low-power irradiation of the water frequency during the relaxation delay (1.3 seconds) for water suppression. Slowly exchanging backbone amide protons of the main chain amide groups were identified by analyses of a series of the HOHAHA spectra recorded at 278 K. Immediately after the lyophilized sample was dissolved in ^2H_2O, the sample was inserted into the pre-shimmed NMR probe, and four sets of 4 hour HOHAHA experiments were carried out. Processing and analyses of the spectra were done using the Bruker XWINNMR and ANSIG programs.[52]

Structure calculations

Interproton distance constraints were obtained from the NOESY spectra recorded with mixing times of 80 ms, 150 ms, and 250 ms. The observed NOE data were classified into four distance ranges, 1.8–2.7 Å, 1.8–3.5 Å, 1.8–5.0 Å, and 1.8–6.0 Å, corresponding to strong,

medium, weak, and very weak NOEs, respectively. Pseudo-atoms were used for the methyl protons or the non-stereospecifically assigned methylene and aromatic protons.[53] Correcting factors for the use of pseudo-atoms were added to the distance constraints. In addition, 0.5 Å was added to the distance constraints involving methyl protons.[54]

Backbone dihedral angle constraints were determined from the backbone NH–C^{α}H coupling constants ($^3J_{N\alpha}$), which were estimated on the DQF-COSY spectrum. The residues with $^3J_{N\alpha} < 5.5$ Hz were constrained to $\phi = [-90°, -40°]$, and the residues with $^3J_{N\alpha} > 8.0$ Hz were constrained to $\phi = [-160°, -80°]$. To determine the χ^1 torsion angle constraints, the $C^{\alpha}H$–$C^{\beta}H$ coupling constants ($^3J_{\alpha\beta}$) estimated from the E.COSY spectrum and the intensity of the intraresidue NOE (H^{α}–H^{β}, HN–H^{β}) were used. Each residue was classified into three rotamers, according to the patterns of the $^3J_{\alpha\beta}$ coupling constants and the intensity of the intraresidue NOE (H^{α}–H^{β}, HN–H^{β}).[55,56] Residues that were classified into g^2g^3, g^2t^3, and t^2g^3 were constrained to $\chi^1 = [0°, 120°]$, $[120°, 240°]$, and $[-120°, 0°]$, respectively. The stereospecific assignments were also established for the β-methylene protons of these residues.

The structural calculation was carried out with the X-PLOR ver 3.1 program.[57] The starting structures, with randomized backbone φ and ψ torsion angles and randomized initial velocities for atoms, were energetically optimized with two simulated annealing protocols: the "dgsa" protocol and the following "refine" protocol.

The disulfide bonding pattern and the hydrogen bond acceptors for the slowly exchanging amide protons of GrTx were identified during the structural determination process. First, to determine the disulfide pairing of GrTx, the initial run of the structural calculation was performed with ambiguous distance restraints between the S^{γ} atoms, according to the strategy proposed by Nilges.[58] After the disulfide pattern was determined by the procedure, the S^{γ} atoms within the disulfide bridges were subjected to a constraint to the target values of 2.0–2.04 Å throughout the structural calculation, except for the refinement process where they are covalently attached to each other.

We then examined the obtained structure to identify the hydrogen bond acceptor for the slowly exchanged amide protons. This procedure was carried out according to the strategy proposed by Fletcher *et al.*[59,60] The target distance constraint values for the determined hydrogen bonds are 1.8–2.3 Å for HN(i)–O(j) and 2.3–3.3 Å for N(i)–O(j).

Final structural calculations were performed on all interproton distance constraints derived from the NOESY spectra, all dihedral angle constraints derived from the coupling constants (DQF-COSY and E.COSY experiments) and NOE measurements, the hydrogen-bond restraints derived from the H–D exchange experiments, and the disulfide bond restraints, which initially were used as ambiguous restraints. We ran the 100 sets of the final structural calculations with all of the determined structural constraints, and chose the 20 best structures based on the X-PLOR energy for structural analysis. The structures were analyzed using the PROCHECK-NMR[61] and MOLMOL programs.[62] The solvent accessible surface areas for the side-chains of amino acid residues were calculated with the solvent radius of 1.4 Å using MOLMOL program. Structural Figures were generated using the MOLMOL program.

Protein Data Bank accession code

The coordinates of GrTx have been deposited in the PCSB Protein Data Bank, accession code 1KOZ.

Acknowledgments

This work was supported by a grant from the Japan New Energy and Industrial Technology Development Organization (NEDO).

References

1. French, R. J. & Dudley, S. C., Jr (1999). Pore-blocking toxins as probes of voltage-dependent channels. *Methods Enzymol.* **294**, 575–605.
2. Bontems, F., Roumestand, C., Gilquin, B., Ménez, A. & Toma, F. (1991). Refined structure of charybdotoxin: common motif in scorpion toxin and insect defensins. *Science*, **254**, 1521–1523.
3. Krezel, A., Kasibhatla, C., Hidalgo, P., MacKinnon, R. & Wagner, G. (1995). Solution structure of the potassium channel inhibitor agitoxin 2: caliper for probing channel geometry. *Protein Sci.* **4**, 1478–1489.
4. Pallaghy, P. K., Duggan, B. M., Pennington, M. W. & Norton, R. S. (1993). Three-dimensional structure in solution of the calcium channel blocker omega-conotoxin. *J. Mol. Biol.* **234**, 405–420.
5. Skalicky, J. J., Metzler, W. J., Ciesla, D. J., Galdes, A. & Pardi, A. (1993). Solution structure of the calcium channel antagonist omega-conotoxin GVIA. *Protein Sci.* **2**, 1591–1603.
6. Davis, J. H., Bradley, E. K., Miljanich, G. P., Nadasdi, L., Ramachandran, J. & Basus, V. J. (1993). Solution structure of omega-conotoxin GVIA using 2-D NMR spectroscopy and relaxation matrix analysis. *Biochemistry*, **32**, 7396–7405.
7. Farr-Jones, S., Miljanich, G. P., Nadasdi, L., Ramachandran, J. & Basus, V. J. (1995). Solution structure of omega-conotoxin MVIIC, a high affinity ligand of P-type calcium channels, using 1H NMR spectroscopy and complete relaxation matrix analysis. *J. Mol. Biol.* **248**, 106–124.
8. Kohno, T., Kim, J. I., Kobayashi, K., Kodera, Y., Maeda, T. & Sato, K. (1995). Three-dimensional structure in solution of the calcium channel blocker omega-conotoxin MVIIA. *Biochemistry*, **34**, 10256–10265.
9. Basus, V. J., Nadasdi, L., Ramachandran, J. & Miljanich, G. P. (1995). Solution structure of omega-conotoxin MVIIA using 2D NMR spectroscopy. *FEBS Letters*, **370**, 163–169.
10. Lu, Z. & MacKinnon, R. (1997). Purification, characterization, and synthesis of an inward-rectifier K^+ channel inhibitor from scorpion venom. *Biochemistry*, **36**, 6936–6940.
11. Srocker, M. & Miller, C. (1994). Electrostatic distance geometry in a K^+ channel vestibule. *Proc. Natl Acad. Sci. USA*, **91**, 9509–9513.
12. Stampe, P., Kolmakova-Partensky, L. & Miller, C. (1994). Intimations of K^+ channel structure from a complete functional map of the molecular surface of charybdotoxin. *Biochemistry*, **33**, 443–450.
13. Hidago, P. & MacKinnon, R. (1995). Revealing the architecture of a K^+ channel pore through mutant cycles with a peptide inhibitor. *Science*, **268**, 307–310.

14. Ranganathan, R., Lewis, J. H. & MacKinnon, R. (1996). Spatial localization of the K^+ channel selectivity filter by mutant cyale-based structure analysis. *Neuron*, **16**, 131–139.
15. Aiyar, J., Withka, J. M., Rizzi, J. P., Singleton, D. H., Andrew, G. C., Lin, W. *et al.* (1996). Topology of the pore-region of a K^+ channel revealed by the NMR-derived structures of scorpion toxins. *Neuron*, **15**, 1169–1181.
16. Naranjo, D. & Miller, C. (1996). A strongly interacting pair of residues on the contact surface of charybdotoxin and a shaker K^+ channel. *Neuron*, **16**, 123–130.
17. Nielsen, K. J., Thomas, L., Lewis, R. J., Alewood, P. F. & Craik, D. J. (1996). A consensus structure for omega-conotoxins with different selectivities for voltage-sensitive calcium channel subtypes: comparison of MVIIA, SVIB and SNX-202. *J. Mol. Biol.* **263**, 297–310.
18. Lew, M. J., Flinn, J. P., Pallaghy, P. K., Murphy, R., Whorlow, S. L., Wright, C. E. *et al.* (1997). Structure–function relationships of omega-conotoxin GVIA. Synthesis, structure, calcium channel binding, and functional assay of alanine-substituted analogues. *J. Biol. Chem.* **272**, 12014–12023.
19. Nielsen, K. J., Adams, D., Thomas, L., Bond, T., Alewood, P. F., Craik, D. J. & Lewis, R. J. (1999). Structure–activity relationships of omega-conotoxins MVIIA, MVIIC and 14 loop splice hybrids at N and P/Q-type calcium channels. *J. Mol. Biol.* **289**, 1405–1421.
20. Swartz, K. J. & MacKinnon, R. (1997). Hanatoxin modifies the gating of a voltage-dependent K^+ channel through multiple binding sites. *Neuron*, **18**, 665–673.
21. Swartz, K. J. & MacKinnon, R. (1997). Mapping the receptor site for hanatoxin, a gating modifier of voltage-dependent K^+ channels. *Neuron*, **18**, 675–682.
22. Li-smerin, Y. & Swartz, K. J. (2000). Localization and molecular determinant of the hanatoxin receptors on the voltage-sensing domain of a K^+ channel. *J. Gen. Physiol.* **115**, 673–684.
23. Rogers, J. C., Qu, Y., Tanada, T. N., Scheuer, T. & Catterall, W. A. (1996). Molecular determinants of high affinity binding of alpha-scorpion toxin and sea anemone toxin in the S3–S4 extracellular loop in domain IV of the Na^+ channel alpha subunit. *J. Biol. Chem.* **271**, 15950–15962.
24. Winterfield, J. R. & Swartz, K. J. (2000). A hot spot for the interaction of gating modifier toxins with voltage-dependent ion channels. *J. Gen. Physiol.* **116**, 637–644.
25. Jablonsky, M. J., Watt, D. D. & Krishna, N. R. (1995). Solution structure of an old world-like neurotoxin from the venom of the new world scorpion *Centruroides sculpturatus* Ewing. *J. Mol. Biol.* **248**, 449–458.
26. Manoleas, N. & Norton, R. S. (1994). Three-dimensional structure in solution of neurotoxin III from the sea anemone *Anemonia sulcata*. *Biochemistry*, **33**, 11051–11061.
27. Swartz, K. J. & MacKinnon, R. (1995). An inhibitor of the Kv2.l potassium channel isolated from the venom of a Chilean tarantula. *Neuron*, **15**, 941–949.
28. Takahashi, H., Kim, J. I., Min, H. J., Sato, K., Swartz, K. J. & Shimada, I. (2000). Solution structure of Hanatoxin1, a gating modifier of voltage-dependent K^+ channels: common structural features of gating modifier toxins. *J. Mol. Biol.* **297**, 771–801.
29. Lampe, R. A., Defeo, P. A., Davison, M. D., Young, J., Herman, J. L., Spreen, R. C. *et al.* (1993). Isolation and pharmacological characterization of ω-grammotoxin SIA, a novel peptide inhibitor of neuronal voltage-sensitive calcium channel responses. *Mol. Pharmacol.* **44**, 451–460.
30. Piser, T. M., Lampe, R. A., Keith, R. A. & Thayer, S. A. (1995). ω-Grammotoxin SIA blocks multiple, voltage-gated, Ca^{2+} channel subtypes in cultured rat hippocampal neurons. *Mol. Pharmacol.* **48**, 131–139.
31. McDonough, S. I., Lampe, R. A., Keith, R. A. & Bean, B. P. (1997). Voltage-dependent inhibition of N- and P-type calcium channels by peptide toxin ω-grammotoxin SIA. *Mol. Pharmacol.* **52**, 1095–1104.
32. Li-Smerin, Y. & Swartz, K. J. (1998). Gating modifier toxins reveal a conserved structural motif in voltage-gated Ca^{2+} and K^+ channels. *Proc. Natl Acad. Sci. USA*, **95**, 8585–8589.
33. Wüthrich, K. (1986). *NMR of Proteins and Nucleic Acids*, Wiley, New York.
34. Richardson, S. J. (1981). The anatomy and taxonomy of protein structure. *Advan. Protein Chem.* **34**, 168–339.
35. Adams, M. E., Mintz, I. M., Reily, M. D., Thanabal, V. & Bean, B. P. (1993). Structure and properties of omega-agatoxin IVB, a new antagonist of P-type calcium channels. *Mol. Pharmacol.* **44**, 681–688.
36. Yu, H., Rosen, M. K., Saccomano, N. A., Phillips, D., Volkmann, R. A. & Schreiber, S. L. (1993). Sequential assignment and structure determination of spider toxin omega-Aga-IVB. *Biochemistry*, **32**, 13123–13129.
37. Kim, J. I., Konishi, S., Iwai, H., Kohno, T., Gouda, H., Shimada, I. *et al.* (1995). Three-dimensional solution structure of the calcium channel antagonist omega-agatoxin IVA: consensus molecular folding of calcium channel blockers. *J. Mol. Biol.* **250**, 659–671.
38. Reily, M. D., Thanabal, V. & Adams, M. E. (1995). The solution structure of omega-Aga-IVB, a P-type calcium channel antagonist from venom of the funnel web spider, *Agelenopsis aperta*. *J. Biomol. NMR*, **5**, 122–132.
39. Burley, S. K. & Petsko, G. A. (1985). Aromatic–aromatic interaction: a mechanism of protein structure stabilization. *Science*, **229**, 23–28.
40. Singh, J. & Thornton, J. M. (1985). The interaction between phenylalanine rings in proteins. *FEBS Letters*, **191**, 1–6.
41. Keith, R. A., Mangano, T. J., Lampe, R. A., DeFeo, P. A., Hyde, M. J. & Donzanti, B. A. (1995). Comparative actions of synthetic omega-grammotoxin SIA and synthetic omega-Aga-IVA on neuronal calcium entry and evoked release of neurotransmitters *in vitro* and *in vivo*. *Neuropharmacology*, **34**, 1515–1528.
42. Mori, Y., Friedrich, T., Kim, M. S., Mikami, A., Nakai, J., Ruth, P. *et al.* (1991). Primary structure and functional expression from complementary DNA of a brain calcium channel. *Nature*, **350**, 398–402.
43. Pragnell, M., Sakamoto, J., Jay, S. D. & Campbell, K. P. (1991). Cloning and tissue-specific expression of the brain calcium channel beta-subunit. *FEBS Letters*, **291**, 253–258.
44. Ellis, S. B., Williams, M. E., Ways, N. R., Brenner, R., Sharp, A. H., Leung, A. T. *et al.* (1988). Sequence and expression of mRNAs encoding the alpha 1 and alpha 2 subunits of a DHP-sensitive calcium channel. *Science*, **241**, 1661–1664.
45. Wei, X. Y., Perez-Reyes, E., Lacerda, A. E., Schuster, G., Brown, A. M. & Birnbaumer, L. (1991). Heterologous regulation of the cardiac Ca^{2+} channel alpha

1 subunit by skeletal muscle beta and gamma subunits. Implications for the structure of cardiac L-type Ca^{2+} channels. *J. Biol. Chem.* **266**, 21943–21947.
46. Rance, M., Sørensen, O. W., Bodenhausen, G., Wagner, G., Ernst, R. R. & Wüthrich, K. (1983). Improved spectral resolution in COSY ^{1}H NMR spectra of protein *via* double quantum filtering. *Biochem. Biophys. Res. Commun.* **117**, 479–485.
47. Griesinger, C., Sørensen, O. W. & Ernst, R. R. (1987). Practical aspects of the E.COSY technique. Measurement of scalar spin–spin coupling constants in peptides. *J. Magn. Reson.* **75**, 474–492.
48. Bax, A. & Davis, D. G. (1985). MLEV-17-based two-dimensional homonuclear magnetization transfer spectroscopy. *J. Magn. Reson.* **65**, 335–360.
49. Jeener, J., Meier, B. N., Bachmann, P. & Ernst, R. R. (1979). Investigation of exchange processes by two-dimensional NMR spectroscopy. *J. Chem. Phys.* **71**, 4546–4553.
50. Macura, S., Huang, Y., Suter, D. & Ernst, R. R. (1981). Two-dimensional chemical exchange and cross-relaxation spectroscopy of coupled nuclear spins. *J. Magn. Reson.* **43**, 259–281.
51. Piotto, M., Saudek, V. & Sklenar, V. (1992). Gradient-tailored excitation for single quantum spectroscopy of aqueous solutions. *J. Biomol. NMR*, **2**, 661–665.
52. Kraulis, P. J. (1989). ANSIG: a program for the assignment of protein ^{1}H 2D NMR spectra by interactive computer graphics. *J. Magn. Reson.* **84**, 627–633.
53. Wüthrich, K., Billeter, M. & Braun, W. (1983). Pseudo-structures for the 20 common amino acids for use in studies of protein conformations by measurement of intramolecular proton–proton distance constraints with nuclear magnetic resonance. *J. Mol. Biol.* **169**, 949–961.
54. Clore, M., Gronenborn, A. M., Nilges, M. & Ryan, C. A. (1987). Three-dimensional structure of potato carboxypeptidase inhibitor in solution. A study using nuclear magnetic resonance, distance geometry and restraint molecular dynamics. *Biochemistry*, **26**, 8012–8023.
55. Hyberts, S. G., Marki, W. & Wagner, G. (1987). Stereospecific assignments of side-chain protons and characterization of torsion angles in Eglin *c*. *Eur. J. Biochem.* **164**, 625–635.
56. Wagner, G., Braun, W., Havel, T. F., Schaumann, T., Go, N. & Wüthrich, K. (1987). Protein structures in solution by nuclear magnetic resonance and distance geometry. The polypeptide fold of the basic pancreatic trypsin inhibitor determined using two different algorithms, DISGEO and DISMAN. *J. Mol. Biol.* **196**, 611–639.
57. Brünger, A. T. (1993). *X-PLOR Manual, Version 3.1*, Yale University, New Haven, CT.
58. Nilges, M. (1995). Calculation of protein structure with ambiguous distance restraints. Automated assignment of ambiguous NOE crosspeaks and disulphide connectivities. *J. Mol. Biol.* **245**, 645–660.
59. Fletcher, J. I., Smith, R., O'Donoghue, S. I., Nilges, M., Conner, M., Howden, M. E. H. *et al.* (1997). The structure of novel insecticidal neurotoxin, omega-atracotoxin-HV1, from the venom of an Australian funnel web spider. *Nature Struct. Biol.* **4**, 559–566.
60. Fletcher, J. I., Chapman, B. E., Mackay, J. P., Howden, M. E. H. & King, G. F. (1997). The structure of versutoxin (δ-atracotoxin-HV1) provides insight into the binding site of site 3 neurotoxins to the voltage-gated sodium channel. *Structure*, **5**, 1525–1535.
61. Laskowski, R. A., Rullmann, J. A., MacArthur, M. W., Kaptein, R. & Thornton, J. M. (1996). AQUA and PROCHECK-NMR: programs for checking the quality of protein structures solved by NMR. *J. Biomol. NMR*, **8**, 477–486.
62. Koradi, R., Billeter, M. & Wüthrich, K. (1996). MOLMOL: a program for display and analysis of macromolecular structures. *J. Mol. Graph.* **14**, 29–32.
63. Brooks, B. R., Bruccoleri, R. E., Olafson, B. D., States, D. J., Swaminathan, S. & Karplus, M. (1983). CHARMm: a program for macromolecular energy, minimization, and dynamics calculations. *J. Comput. Chem.* **4**, 187–217.

Edited by M. F. Summers

(Received 27 March 2002; received in revised form 11 June 2002; accepted 12 June 2002)